

# Applicability of a single-particle picture for resonant photoelectron spectroscopy on molecule-metal interfaces

C. Sauer, M. Wießner, A. Schöll, and F. Reinert

*Universität Würzburg, Experimentelle Physik VII & Röntgen Research Center for Complex Material Systems RCCM, 97074 Würzburg, Germany*

(Received 17 August 2015; revised manuscript received 7 December 2015; published 4 January 2016)

In this paper we discuss how far a single-particle picture can be applied for the description of photoelectron spectroscopy of large  $\pi$ -conjugated molecules on metal substrates measured near a  $K$  edge. In this context we focus on particular spectroscopic features, which only exist at the immediate interface and show a constant kinetic energy when the photon energy is varied immediately above a resonance. We demonstrate that the kinetic energy of these features can be calculated on the basis of a single-particle picture for molecule-metal interface systems without charge transfer in the ground state. Similar features are also observed in the case of molecule-metal interfaces which show an occupation of the formerly lowest unoccupied molecular orbital in direct photoelectron spectroscopy as a result of charge transfer in the ground state. However, an analogous calculation of the kinetic energy of these signals fails here, indicating that a single-particle picture is not sufficient for these systems, for which many-body effects have to be adequately taken into account.

DOI: [10.1103/PhysRevB.93.045101](https://doi.org/10.1103/PhysRevB.93.045101)

## I. INTRODUCTION

In many studies the description of resonant photoelectron spectroscopy (RPES) relies on the single-particle picture. This usually includes schematic diagrams of the involved states for the separated processes of excitation, intermediate state, and deexcitation (see for example Refs. [1–3]). The possibility of charge transfer and the determination of the energy of emitted electrons is hereby discussed on the basis of the comparison of single-particle states [4–7]. However, if many-body effects become important, a single-particle picture needs to be extended or it must even be completely dismissed.

A suitable class of systems for an investigation of the applicability and the limits of a single-particle picture for RPES is given by large  $\pi$ -conjugated molecules. By adsorbing the same molecule on different substrates different types of interfaces can be realized. Therefore it is possible to compare the same process within the same molecule in different regimes of interface interaction. The criterion we use in this paper to distinguish between two different types of molecule-metal interface systems is the existence of charge transfer in the ground state between the substrate and the adsorbate. In the case of the systems in the following, this charge transfer occurs from the metal substrate to the adsorbate molecules and manifests itself in a signal originating from the lowest unoccupied molecular orbital (LUMO) of the free molecule in direct photoelectron spectroscopy (PES) [8–10]. Recent experiments prove that electron correlations can play an important role in such cases [11–14]. Hence the applicability of the single-particle picture for the description of RPES on these systems is questionable.

In previous RPES studies of molecule-metal interface systems without ground state charge transfer, organic heterointerfaces, and multilayer systems [15,16], a resonant enhancement of molecular orbital signals was observed, and their photon energy ( $h\nu$ ) dependent line-shape evolution was explained by electron-vibration coupling. Hence in RPES on such molecule-metal interface systems some effects are well described by a comparison to small molecules (e.g., CO, N<sub>2</sub>, O<sub>2</sub>, and OCS) in the gas phase [17–20]. Consequently,

here the consideration of an isolated molecule can still be appropriate for the description of the spectra. On the other hand, in the RPES data of coronene/Ag(111) we have recently reported the discovery of a characteristic feature at low binding energy ( $E_B$ ), which can be assigned to a particular final state involving charge transfer on the basis of a cluster model [21]. Hence for coronene/Ag(111), which does not show significant charge transfer in the ground state, a treatment of RPES equivalent to strongly correlated transition metal compounds [22,23] can be justified. Furthermore, the above mentioned low  $E_B$  feature exhibits a particular line shape which is characteristic for molecular orbital signals at interfaces with strong hybridization and ground state charge transfer [21]. This demonstrates that for the description of a particular feature in the RPES data a single-particle picture might be inappropriate although some aspects of direct valence PES of the same system can still be discussed by considering an isolated molecule [24].

In this paper we address the question of the applicability of a single-particle picture for RPES on selected molecule-metal interface systems. For that features in the RPES data, which appear at constant kinetic energy ( $E_K$ ) above a resonance, are quantitatively analyzed. First we show that within the single-particle picture that the kinetic energy of these features can be successfully calculated for molecule-metal interfaces which do not show charge transfer in the ground state [e.g., tin-phthalocyanine (SnPc) on Au(111) and coronene on Ag(111)]. We then demonstrate that the same approach fails in the case of molecule-metal systems with a considerable charge transfer in the ground state [e.g., copper-phthalocyanine (CuPc) on Ag(111)]. We draw the conclusion that in the latter case many-body interactions need to be taken into account for a proper description of the RPES data.

## II. EXPERIMENTAL

RPES, PES, and near-edge x-ray absorption fine structure (NEXAFS) measurements were performed at BESSY II at the undulator beamline UE52-PGM ( $E/\Delta E > 14000$  at 400 eV

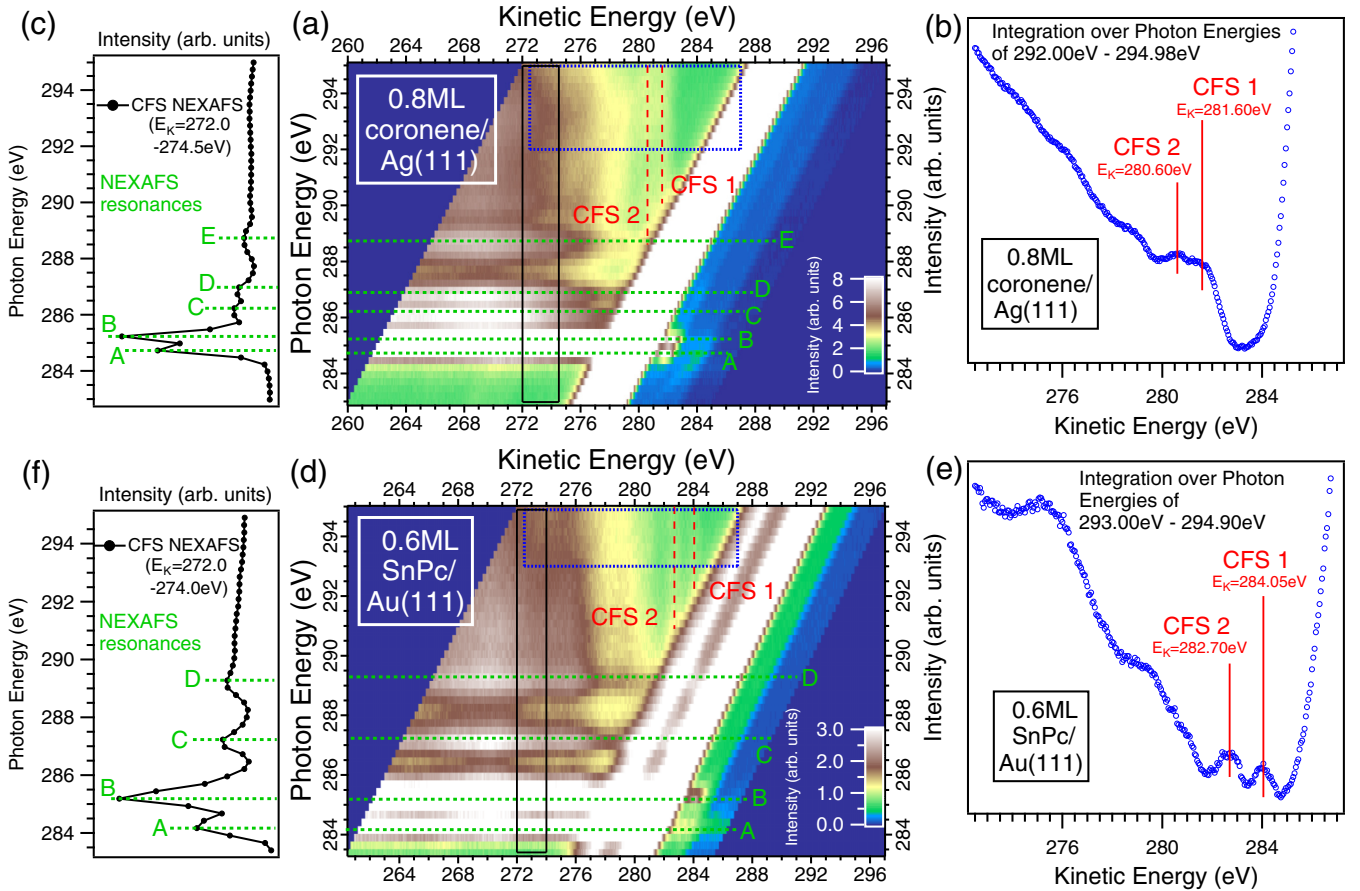


FIG. 1. RPES data of 0.8 ML coronene/Ag(111) [upper panels (a)–(c)] and 0.6 ML SnPc/Au(111) [lower panels (d)–(f)] recorded at the carbon  $K$  edge. The middle panels show the intensity maps on a kinetic energy scale. On the right hand side [(b) and (e)] EDCs derived from integrating the area inside the dashed blue lines of the maps [(a) and (d)] over photon energy are presented (for details see text). The intensities were scaled to allow the observation of the constant  $E_K$  features, which are marked in the maps [middle panels, (a) and (d)] by dashed red lines. On the left hand side [(c) and (f)] NEXAFS spectra extracted by integration over  $E_K$  within the black box of the maps [(a) and (d)] are displayed (for details see text). The NEXAFS resonances are marked in the RPES maps [(a) and (d)] by dashed green lines.

photon energy, with  $\text{cfl} = 10$  and  $20 \mu\text{m}$  exit slit [25]) at room temperature in a UHV chamber with a pressure below  $5 \times 10^{-10}$  mbar. All spectra were recorded with  $p$ -polarized light with a  $70^\circ$  angle of incidence with respect to the surface normal, a beamline exit slit of  $40 \mu\text{m}$ , and a  $\text{cfl}$  value of 10, resulting in an energy resolution of better than 40 meV at 300 eV photon energy. Core level PES data were measured in the same beamline settings but in normal emission geometry ( $55^\circ$  angle of incidence with respect to the surface normal). RPES and PES photoelectron intensities were detected with a Scienta R4000 electron analyzer which was operated with an entrance slit of  $300 \mu\text{m}$ . PES core level data were measured with a pass energy of 20 eV and valence regime data with a pass energy of 50 eV which results in an energy resolution of  $\Delta E = 30$  meV and  $\Delta E = 75$  meV, respectively. For the RPES maps [see Figs. 1(a) and 1(d) and Figs. 3(a) and 3(d)] a pass energy of 100 eV was used resulting in an energy resolution of  $\Delta E = 150$  meV. The energy distribution curves (EDC) in Fig. 4(b) were derived from more detailed RPES maps recorded with a pass energy of 50 eV and  $\Delta E = 75$  meV. The NEXAFS spectra in Figs. 2 and 4 were measured with a partial electron yield detector using a retarding voltage of 150 V.  $h\nu$  (and  $E_B$ ) were calibrated according to Ref. [26]. RPES

and NEXAFS intensities were normalized to the ring current and the beamline flux curve which was recorded separately by measuring the  $h\nu$  dependence of the intensity of a PES signal of the clean surface (RPES) or the same partial electron yield signal as for the actual measurement (NEXAFS) [26].

The Ag(111) and Au(111) substrates were cleaned by several sputter and annealing cycles, and their cleanliness was confirmed by PES. All organic materials were purified by sublimation and evaporated from home built Knudsen cells at pressures below  $10^{-8}$  mbar onto the room temperature substrates. Film thickness was determined by core level PES intensities of the adsorbate, using the effective electron attenuation lengths given in Ref. [27], and the emergence of characteristic features stemming from a particular adsorbate layer. The samples were carefully checked for radiation damage especially after the RPES data acquisition.

### III. RESULTS AND DISCUSSION

In comparison to off-resonant (or direct) PES, an additional criterion to classify signals arises in RPES due to the variation of the photon energy. There are two main possibilities for an apparent spectral feature to disperse with  $h\nu$ : It can either

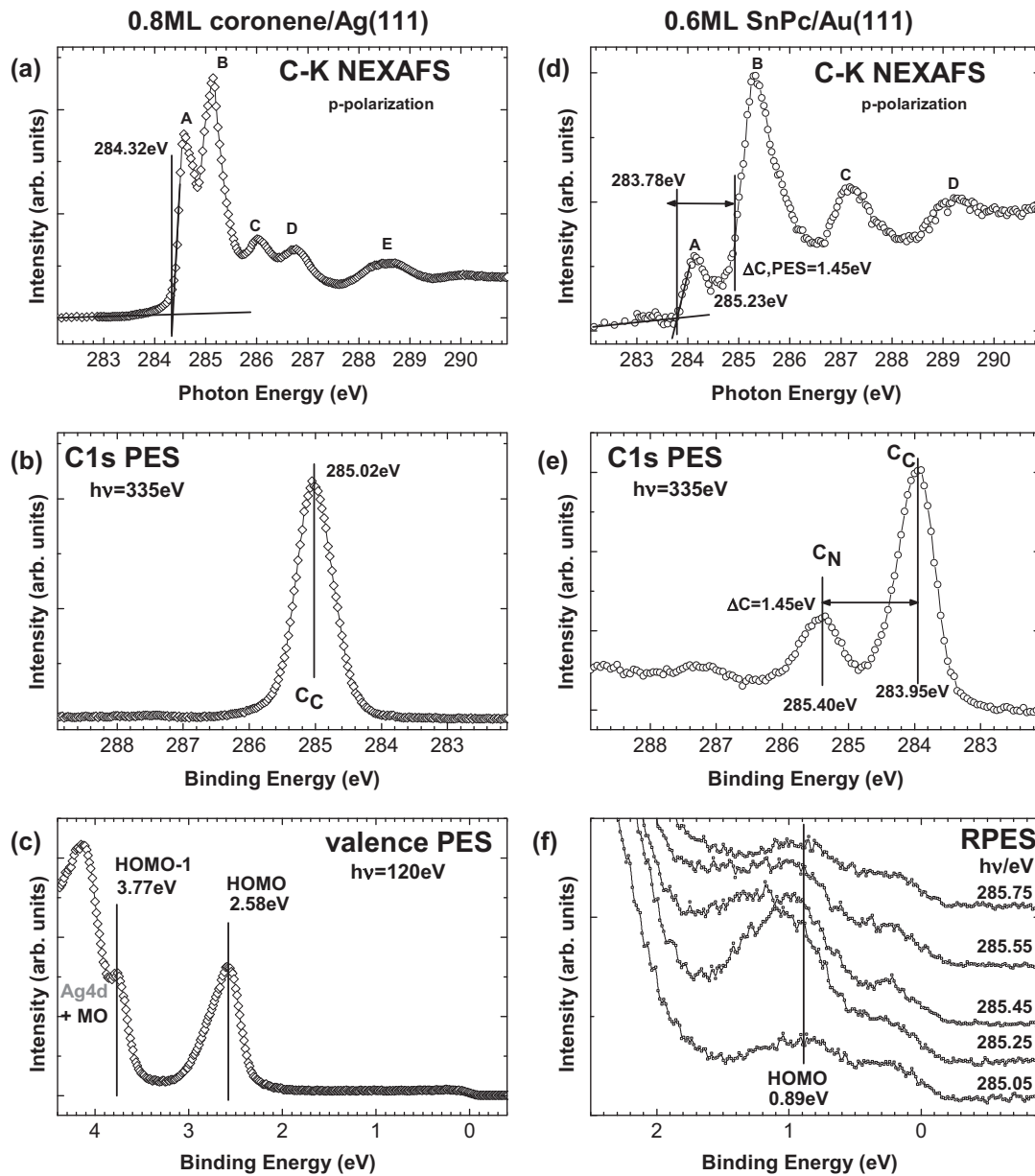


FIG. 2. Carbon *K*-edge (C-*K*) NEXAFS data [top panels (a) and (d)] recorded with *p* polarization, C1s core level PES spectra [middle panels (b) and (e)] and valence PES spectra [bottom panels (c) and (f)] of 0.8 ML coronene/Ag(111) [left hand side (a)–(c)] and 0.6 ML SnPc/Au(111) [right hand side (d)–(f)]. The capital letters denote the NEXAFS resonances (see also Fig. 1) and the black lines illustrate the determination of the NEXAFS onset. From both C1s PES spectra [middle panels (b) and (e)] a power law background was subtracted. C<sub>C</sub> and C<sub>N</sub> represent the energy position of the C1s species bound to carbon and nitrogen, respectively. For 0.6 ML SnPc/Au(111) the extracted difference for the two C1s species ( $\Delta C$ ) [bottom right (e)] is also shown in the NEXAFS spectrum [top right (d)] to determine the NEXAFS onset corresponding to the C<sub>N</sub> carbon species (for details see text). The valence PES of coronene/Ag(111) in (c) was recorded with a photon energy of 120 eV. The binding energy of the HOMO was derived from the peak maximum as indicated by the horizontal line. (f) displays selected EDCs from the RPES data in Fig. 1(d) at the indicated photon energies. The HOMO binding energy is determined from the low energy component as indicated by the horizontal line (for details see text).

stay at constant binding energy or linearly disperse to higher binding energy with increasing  $h\nu$  because of its constant kinetic energy. In the former case the  $h\nu$  dependence of these features is measured as so-called constant initial state (CIS) spectra, while in the latter case these are constant final state (CFS) spectra. The principle that allows a reasonable characterization of features at constant  $E_B$  and at constant  $E_K$  is energy conservation including the photon in the initial

state. In other words constant  $E_B$  features stem from a coherent process in which the energy and the quantum mechanical phase are conserved. In contrast to that constant  $E_K$  features occur when the kinetic energy of the photoelectron is independent of the photon energy. This means that only the energy difference of the states involved in autoionization or an Auger decay determine the kinetic energy of the emitted electron which hence remains constant for the same process. Correspondingly,

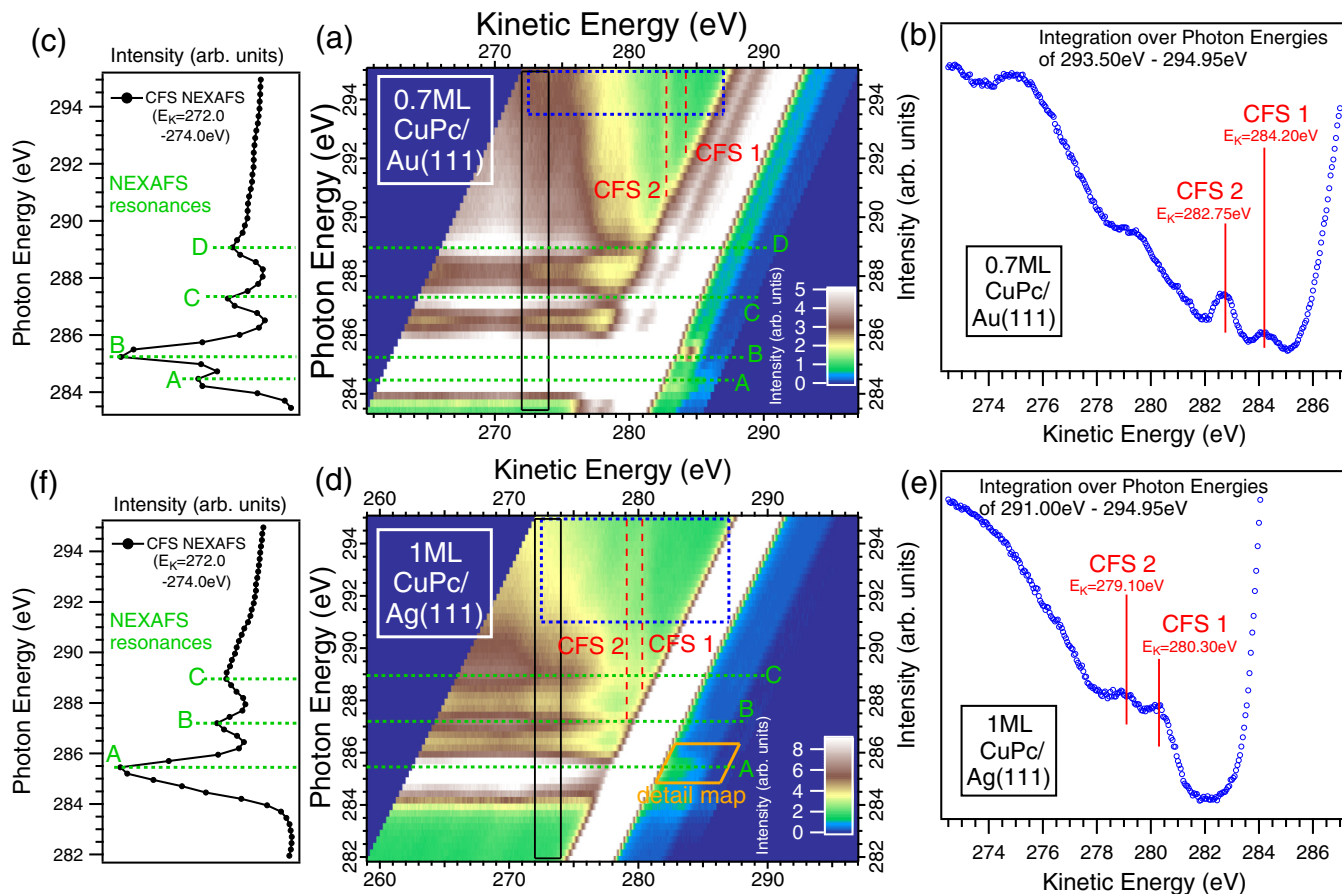


FIG. 3. RPES data of 0.7 ML CuPc/Au(111) [upper panels (a)–(c)] and 1 ML CuPc/Ag(111) [lower panels (d)–(f)] at the carbon  $K$  edge. The middle panels show the RPES maps on an  $E_K$  scale. The orange box in the 1 ML CuPc/Ag(111) RPES map [lower middle panel (d)] denotes the area from which the EDCs presented in Fig. 4(b) originate. On the right hand side EDCs derived from integrating over photon energy in the area inside the dashed blue lines of the RPES maps [(a) and (d)] are presented (for details see text). The identified constant  $E_K$  features are marked in the RPES maps [middle panels (a) and (d)] by dashed red lines. On the left hand side [(c) and (f)] NEXAFS spectra extracted by integration over  $E_K$  within the black box of the RPES maps [(a) and (d)] are displayed (for details see text). The NEXAFS resonances are marked in the RPES maps [(a) and (d)] by dashed green lines.

there are two different ways to present RPES data, namely on a binding or on a kinetic energy scale ( $E_B = h\nu - E_K$ ). Whenever the focus lies on constant  $E_K$  features, a kinetic energy scale is more reasonable since it facilitates the observation of such signals. Thus the PES intensity maps in Figs. 1 and 3 show the photon energy dependent photoemission intensity of coronene on Ag(111) [Fig. 1(a)], SnPc on Au(111) [Fig. 1(d)], as well as of CuPc on Au(111) [Fig. 3(a)] and on Ag(111) [Fig. 3(d)] plotted against kinetic energy.

In each of the RPES data sets presented in Figs. 1 and 3, two particular signals at constant kinetic energy are clearly observed for photon energies immediately above the resonant transitions A–E. These signals are indicated by the vertical dashed red lines and denominated CFS1 and CFS2. Note that such signals also occur for 1 ML SnPc/Ag(111) [28] and 1 ML NTCD/Ag(111) (Ref. [29] and additional measurements not shown). For a quantitative determination of the energy of these peaks, the area within the blue dashed lines was integrated in the  $h\nu$  direction. This has the consequence that signals at constant binding energy smear out since they disperse while the intensities at constant  $E_K$  add up. The resulting integrated energy distribution curves (EDC) are presented in Figs. 1(b)

and 1(e) as well as Figs. 3(b) and 3(e). Note that the photon energy regions for integration were chosen to avoid a crossing of the intense substrate bands (Ag4d and Au5d, respectively), and thus this region varies for the different substrates. Panels (c) and (f) on the left hand side of Figs. 1 and 3 show the NEXAFS spectra obtained from an integration in kinetic energy direction in the area indicated by the black boxes of the corresponding PES overview maps.

#### A. General discussion of constant kinetic energy features

The absence of the constant  $E_K$  features described above for multilayer samples and for the bare substrates identifies them as interface originated. Similar signals have previously been observed for two other systems [5,6], and these have also been attributed to the processes at the molecule-metal interface. We will in the following explain the energy of these features quantitatively on the basis of a single-particle picture and identify the responsible decay channel.

We assume that for the molecule-metal interfaces without ground state charge transfer (and thus no LUMO signal in direct valence PES) the overall electronic structure of the molecules at the interface is not significantly altered with

respect to the bulk material. The difference between bulk and monolayer spectra thus must be explained by the importance of metal states at the interface. A detailed discussion about this fact is given in Sec. III C, and we will concentrate on the systems without a LUMO signal in direct valence PES at this point.

The constant  $E_K$  features have in common that the kinetic energy of the highest lying signal (CFS 1) is larger than the largest possible kinetic energy of a regular Auger decay. The latter involves a decay of a core hole in the carbon species with the largest binding energy which produces a final state with two holes in the highest occupied molecular orbital (HOMO). Consequently, this observed excess in kinetic energy indicates the involvement of a molecular state with smaller binding energy than the HOMO in the responsible decay process. Additionally, since the kinetic energy of the constant  $E_K$  features is independent of the photon energy, we can exclude a coherent one-step process (as described in Ref. [21]). Hence we can divide the responsible process into two steps [(a) and (b)], and the observed energy of the emitted electron is the energetic difference of the intermediate state and the final state. If the photon energy is larger than the core level ionization potential, step (a) will correspond to core level PES and step (b) to an Auger decay.

As indicated above the process responsible for the constant  $E_K$  features has to involve a molecular state with smaller binding energy than the HOMO and dynamical charge transfer (CT) in step (a) from the metal to this particular state, which under our assumption of mainly unperturbed molecular states must be the LUMO. In a nomenclature based on the cluster model description of transition metal compounds [22,30–34], basis states can be defined of the form  $|C_i^a H_j^b L_0^c M^d\rangle$  with  $C_i$  representing the C 1s state of carbon site  $i$ ,  $H_j$  the occupied molecular orbital  $j$ ,  $L_0$  the LUMO, and  $M$  a metal state from the conduction band. The superscripts ( $a, b, c, d$ ) denote the integer occupation of the respective state. All states that are not directly involved in the particular process are omitted. In this nomenclature and by considering an initial, an intermediate, and a final state described by the explained basis, the full RPES process can be written for photon energies larger than the ionization potential as

$$\begin{aligned} \text{(a)} & |C_i^2 H_j^2 L_0^0 M^n\rangle + h\nu \xrightarrow{\text{PES}} |C_i^1 H_j^2 L_0^1 M^{n-1}\rangle + e^- \\ \text{(b)} & |C_i^1 H_j^2 L_0^1 M^{n-1}\rangle \xrightarrow{\text{Auger}} |C_i^2 H_j^1 L_0^0 M^{n-1}\rangle + e^-. \end{aligned}$$

Hereby the text above the arrows denotes the particular process. Below the arrow additional dynamical charge transfer from the metal  $M$  to the LUMO  $L_0$  during the time scale of the core hole lifetime in step (a) is indicated. Note that at this point only interfaces without ground state charge transfer are considered, and thus for these systems a significant admixture of a basis state with charge transfer can be excluded in the initial state.

In order to predict the energy of the constant  $E_K$  features, the energy of the basis states with respect to a common reference has to be determined. This is straightforward if the metal states  $M$  can be ignored since then these states become eigenstates of the respective system. If only molecular states are considered the state  $|C_i^1 H_j^2 L_0^1\rangle$  can be measured in

a NEXAFS experiment and the state  $|C_i^2 H_j^1 L_0^0\rangle$  in direct PES, with respect to the state  $|C_i^2 H_j^2 L_0^0\rangle$ . By neglecting the metal states  $M$  we factorize the basis states into a molecular and a metal part so we can cancel out the energy of the latter in the energy balance of step (b). Note that we thus have to assume the overlap of metal and molecular states to be small, but at the same time large enough to enable charge transfer from  $M$  to  $L_0$  either in the initial state or in the intermediate state. If hybridization between molecular and metal states is present, generally excitations including metal states are possible in the final state. Our approximations thus rely on a small hopping matrix element  $V_{L,M}$  between  $M$  and  $L_0$  in the sense of Refs. [35,36].

These approximations can be written in the above notation as follows, which defines the single-particle picture applied in this paper:

$$\begin{aligned} (1) & |C_i^1 H_j^2 L_0^1 M^{n-1}\rangle \approx |C_i^1 H_j^2 L_0^1\rangle \cdot |M^{n-1}\rangle \\ (2) & |C_i^2 H_j^1 L_0^0 M^{n-1}\rangle \approx |C_i^2 H_j^1 L_0^0\rangle \cdot |M^{n-1}\rangle \\ (3) & \text{NEXAFS} \hat{=} |C_i^2 H_j^2 L_0^0\rangle + h\nu \rightarrow |C_i^1 H_j^2 L_0^1\rangle \\ (4) & \text{valence PES} \hat{=} |C_i^2 H_j^2 L_0^0\rangle + h\nu \rightarrow |C_i^2 H_j^1 L_0^0\rangle + e^-. \end{aligned}$$

### B. Successful application of a single-particle picture

The energy of the electronic transitions in the NEXAFS spectra of coronene/Ag(111) and SnPc/Au(111) will be determined from the onset of the respective peaks. This is the best approximation to the energetically lowest adiabatic transitions of the vibrationally broadened signals [37,38].

Coronene consists of three chemically different carbon species which cannot be distinguished in PES [see Fig. 2(b)] due to their small energetic separation. We will thus not distinguish between different carbon species for coronene and only consider a single one denominated  $C_C$  in the following.

The most prominent NEXAFS resonances  $A$  and  $B$  are explained in literature by a lift of the degeneracy of the coronene LUMO following the localized core excitation [39]. The separation of the adiabatic transitions associated with NEXAFS resonances  $A$  and  $B$  can be estimated to be less than 0.5 eV from Fig. 2(a). Even considering error bars this is too small to explain the separation of about 1 eV between CFS1 and CFS2 in Fig. 1(b). We, however, assume that the splitting of the transitions due to the lift of degeneracy cannot be resolved in our data but contributes to the broadening of the signals assigned to CFS1 and 2 in Fig. 1(b), which actually appear slightly broader than the respective features in the case of SnPc/Au(111) in Fig. 1(e).

We rather explain the emergence of the two constant  $E_K$  features in the RPES data of coronene/Ag(111) by the involvement of the HOMO ( $H_0$  corresponding to the basis state  $|C_C^2 H_0^1 L_0^0\rangle$  with  $E_B(|C_C^2 H_0^1 L_0^0\rangle) = 2.58$  eV) for CFS 1 and the HOMO-1 [ $H_{-1}$  corresponding to the basis state  $|C_C^2 H_{-1}^0 L_0^0\rangle$  with  $E_B(|C_C^2 H_{-1}^0 L_0^0\rangle) = 3.77$  eV] for CFS 2. For the determination of the binding energy of these molecular orbitals from the valence PES spectrum in Fig. 2(c), we used the peak maxima as an approximation for the adiabatic transition which constitutes the energy of the final state without a vibronic excitation. The possible error made by this

approximation is determined to be less than 100 meV by a single mode analysis [40].

When using the onset of the NEXAFS peak A as a value for the photon energy of the electronic transitions of all three carbon species into the LUMO, the theoretical value  $E_{\text{theo}}(\text{CFS } m)$  for the kinetic energy of the constant  $E_K$  feature  $m$  is calculated with the following equation

$$E_{\text{theo}}(\text{CFS } m) = h\nu(|C_i^1 H_j^2 L_0^1\rangle) - E_B(|C_i^2 H_j^1 L_0^0\rangle),$$

where  $m$  is the index of the particular peak (i.e., CFS 1 and 2),  $i$  the index of the carbon species, and  $j$  of the involved molecular orbital. For coronene/Ag(111) CFS 1 is identified as the Auger decay of the basis state  $|C_C^1 H_0^2 L_0^1\rangle$  to  $|C_C^2 H_0^1 L_0^0\rangle$ , and its kinetic energy is calculated to

$$\begin{aligned} E_{\text{theo}}(\text{CFS } 1) &= h\nu(|C_C^1 H_0^2 L_0^1\rangle) - E_B(|C_C^2 H_0^1 L_0^0\rangle) \\ &= 284.32 \text{ eV} - 2.58 \text{ eV} = (281.74 \pm 0.20) \text{ eV}. \end{aligned}$$

CFS 2 is attributed to the Auger decay of the basis state  $|C_C^1 H_{-1}^2 L_0^1\rangle$  to  $|C_C^2 H_{-1}^1 L_0^0\rangle$ , and we obtain

$$\begin{aligned} E_{\text{theo}}(\text{CFS } 2) &= h\nu(|C_C^1 H_{-1}^2 L_0^1\rangle) - E_B(|C_C^2 H_{-1}^1 L_0^0\rangle) \\ &= 284.32 \text{ eV} - 3.77 \text{ eV} = (280.55 \pm 0.20) \text{ eV}. \end{aligned}$$

These values are in agreement with the experimentally determined ones in Fig. 1(b) which are

$$\begin{aligned} E_{\text{exp}}(\text{CFS } 1) &= (281.60 \pm 0.15) \text{ eV} \\ E_{\text{exp}}(\text{CFS } 2) &= (280.60 \pm 0.15) \text{ eV}. \end{aligned}$$

The error of the experimental values is due to the reading accuracy, while the theoretical errors stem from the uncertainty of the determination of the adiabatic transitions in the NEXAFS and PES spectra. The agreement of the theoretical and experimental values justifies the approximations we made in explaining the energy of the constant  $E_K$  features. Furthermore, the agreement confirms that the process in step (b) properly describes the origin of these features. Hence the application of the single-particle picture as defined above seems to be appropriate for the description of these features in the data of coronene/Ag(111). Note, however, that the general statement that a single-particle picture is a reasonable approximation for RPES on coronene/Ag(111) is troublesome since the neglected hopping matrix element  $V_{L,M}$  is vital in the discussion in Ref. [21]. The necessity of the consideration of many-body physics in the latter case arises from the fact that a coherent one step process is described there while in the present paper an incoherent two-step process is responsible for the investigated features.

For SnPc we can evaluate the energy of the constant  $E_K$  features analogously. Two different carbon species are considered in this case ( $C_C$  and  $C_N$ ) as denoted in the C1s PES data in Fig. 2(e). The NEXAFS resonances A and B in Fig. 2(d) relevant for the following evaluation can be assigned to transitions from the  $C_C$  and  $C_N$  1s levels to the LUMO [41]. We again use the low energy NEXAFS onset for the determination of the energy of the basis state  $|C_C^1 H_j^2 L_0^1\rangle$  [see Fig. 2(d)]. The corresponding energy of the basis state  $|C_N^1 H_j^2 L_0^1\rangle$  is estimated from the separation of the peaks in the PES spectrum [see Fig. 2(d)] corresponding to the two considered carbon species [42]. For the determination of this

energetic difference the peak maxima are used for simplicity. An evaluation of the peak onsets is complicated for the  $C_N$  peak but would result in a very similar value for the separation of  $C_C$  and  $C_N$ . The result for the NEXAFS onset corresponding to the basis state  $|C_N^1 H_j^2 L_0^1\rangle$  is displayed in Fig. 2(d). This rather crude approximation will be considered in the error of the energy determined for the feature CFS 1 of SnPc. In the case of SnPc/Au(111) the process leading to CFS 1 is identified as the Auger decay from the basis state  $|C_N^1 H_0^2 L_0^1\rangle$  to  $|C_N^2 H_0^1 L_0^0\rangle$ . Unfortunately the determination of the binding energy of the HOMO is not as straightforward as in the case of coronene/Ag(111), because the SnPc HOMO peak intensity is very low in direct PES and in addition the strong background from the Au valence bands complicates the evaluation. A determination of the required value is however possible from the RPES data in Fig. 1(d). Selected EDCs are displayed in the waterfall plot in Fig. 2(f). As we have discussed in detail in a previous publication, the SnPc HOMO shows a variation of the line shape due to vibronic coupling on resonance [16]. The binding energy of  $E_B = 0.89$  eV for the state  $|C_i^2 H_0^1 L_0^0\rangle$  was thus derived from the low energy compound of the HOMO peak as indicated in Fig. 2(f). With these values we obtain

$$\begin{aligned} E_{\text{theo}}(\text{CFS } 1) &= h\nu(|C_N^1 H_0^2 L_0^1\rangle) - E_B(|C_N^2 H_0^1 L_0^0\rangle) \\ &= 285.23 \text{ eV} - 0.89 \text{ eV} = (284.34 \pm 0.30) \text{ eV}. \end{aligned}$$

CFS 2 is then explained by an Auger decay from  $|C_C^1 H_0^2 L_0^1\rangle$  to  $|C_C^2 H_0^1 L_0^0\rangle$ . Hence

$$\begin{aligned} E_{\text{theo}}(\text{CFS } 2) &= h\nu(|C_C^1 H_0^2 L_0^1\rangle) - E_B(|C_C^2 H_0^1 L_0^0\rangle) \\ &= 283.78 \text{ eV} - 0.89 \text{ eV} = (282.89 \pm 0.20) \text{ eV}. \end{aligned}$$

Since no significant PES intensity at the energy position of the HOMO-1 is found in any NEXAFS resonance in the RPES map, a negligible probability for the Auger decay from  $|C_i^1 H_{-1}^2 L_0^1\rangle$  to  $|C_i^2 H_{-1}^1 L_0^0\rangle$  can be concluded. Hence it is reasonable that there are no visible constant  $E_K$  features originating from processes analogous to the ones of CFS 1 and CFS 2 including the HOMO-1. The theoretical values for SnPc/Au(111) are in agreement with the experimental ones

$$\begin{aligned} E_{\text{exp}}(\text{CFS } 1) &= (284.05 \pm 0.10) \text{ eV} \\ E_{\text{exp}}(\text{CFS } 2) &= (282.70 \pm 0.10) \text{ eV} \end{aligned}$$

which are extracted from Fig. 1(e). This seems to justify our approximations, the assignment of step (b) as the responsible process, and the application of the single-particle picture for the description of the constant  $E_K$  features in the data of SnPc/Au(111).

In principle there could be many more constant  $E_K$  features similar to the ones discussed above, if molecular orbitals with larger binding energy were considered for an Auger decay process as in step (b). The fact that these are not observed can be explained in two different ways. One explanation is based on the finding that these lower lying molecular orbitals are energetically closer together than the frontier ones. For coronene/Ag(111) this is explicitly observed and discussed in Ref. [24]. The resulting total signal would then be broad and contain no distinct peak features. Another explanation is that the Auger matrix elements for these decays are simply too small.

### C. Limits of the single-particle picture

In section III B we have demonstrated that a single-particle picture as defined in III A can be applied successfully to calculate the energy of certain constant  $E_K$  features. In this section we show that the same approach fails when it is applied to the respective features found in the data with substantial hybridization and charge transfer in the ground state. In Fig. 3 RPES data of CuPc on Au(111) and on Ag(111) is presented. For CuPc/Au(111), a system without a LUMO signal in direct PES, two constant  $E_K$  features are observed at similar energy as for SnPc/Au(111). The mechanism that is responsible for these features at the CuPc/Au(111) interface is analogous to SnPc/Au(111). The comparison of the data of CuPc on Au(111) and on Ag(111) allows comparing a molecule-metal interface system without and one with ground state charge transfer and reveals a prominent difference. In the latter case the two constant  $E_K$  features are found above resonance at a kinetic energy which is almost 4 eV smaller than in the former. The same situation is also found for the comparison of SnPc/Ag(111) [28] with SnPc/Au(111). At the NTCDA/Ag(111) interface (Ref. [29] and additional measurements not shown) a constant  $E_K$  feature is also observed as a clearly visible peak at similarly small kinetic energy. Hence the low energy of the constant  $E_K$  features seems to be a general effect for the molecule-metal interface systems with a LUMO signal in direct PES.

Simply transforming the mechanism used for the molecule-metal interface systems without to such systems with ground state charge transfer can be done by considering an electron in the state  $L_0$  of the basis state that describes the initial state. Hence after an excitation as in step (a) the basis state  $|C_i^1 H_0^2 L_0^2 M^{n-1}\rangle$  is produced which decays into  $|C_i^2 H_0^1 L_0^1 M^{n-1}\rangle$  as in step (b). Proceeding analogously to Secs. III A and III B, these basis states are separated into a molecular part and a part with the metal states  $M$ . The energy of the state  $|C_i^1 H_0^2 L_0^2\rangle$  is determined from NEXAFS [see Fig. 4(a)] to 284.05 eV and the energy of the state  $|C_i^2 H_0^1 L_0^1\rangle$  from PES [see bottom EDC of Fig. 4(b)] to 1.40 eV. With this  $E_{\text{theo}}(\text{CFS } 2)$  is calculated for 1 ML CuPc/Ag(111) to

$$\begin{aligned} E_{\text{theo}}(\text{CFS } 2) &= h\nu(|C_i^1 H_0^2 L_0^2\rangle) - E_B(|C_i^2 H_0^1 L_0^1\rangle) \\ &= 284.05 \text{ eV} - 1.40 \text{ eV} = (282.65 \pm 0.20) \text{ eV}, \end{aligned}$$

which is 3.55 eV larger than the experimental value  $E_{\text{exp}}(\text{CFS } 2) = (279.10 \pm 0.15) \text{ eV}$  found in Fig. 3(e). The value for the  $C_N$  carbon species,  $E_{\text{theo}}(\text{CFS } 1)$ , differs analogously. Consequently, a mechanism as used for the molecule-metal interface systems without ground state charge transfer [step (b)] in combination with assumptions (1)–(4) cannot explain the observed energy of the constant  $E_K$  features in the case of CuPc/Ag(111). The same applies to the constant  $E_K$  features in the RPES data of SnPc/Ag(111) [28] and of NTCDA/Ag(111) (Ref. [29] and additional measurements not shown), which also cannot be described by the approach presented in Secs. III A and III B. This indicates that the constant  $E_K$  features in the case of interfaces with ground state charge transfer are based on a different mechanism.

For CuPc/Ag(111) such a possible alternative mechanism would be an Auger decay involving the LUMO and a molecular orbital  $H_{-x}$  with  $E_B \approx 5 \text{ eV}$ . This  $C_i H_{-x} L_0$ -Auger decay is

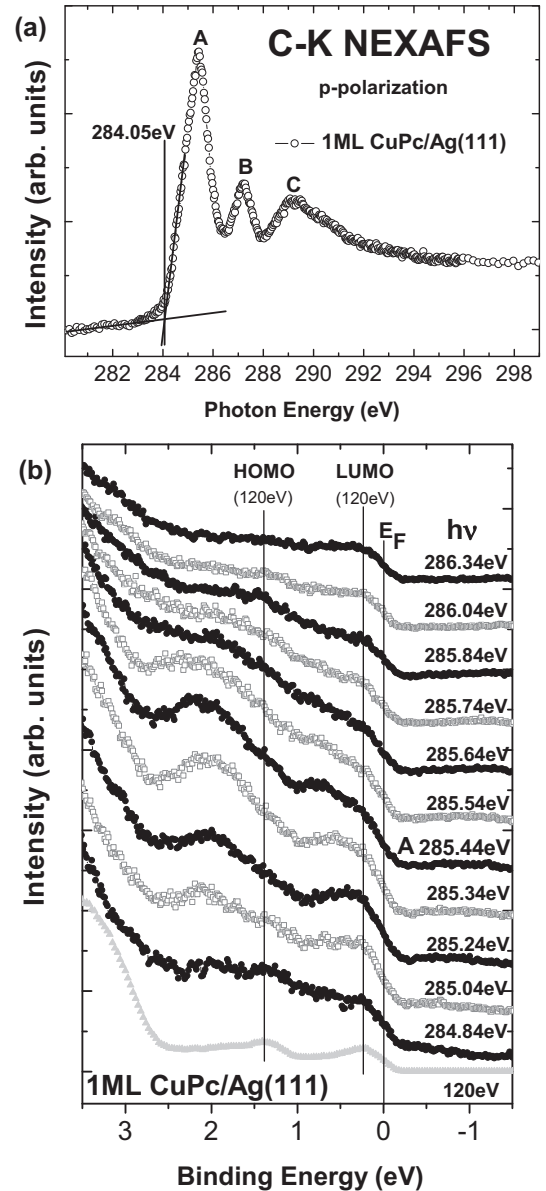


FIG. 4. C-K NEXAFS (a) and RPES (b) data of 1 ML CuPc/Ag(111). The capital letters in (a) denote the NEXAFS resonances, and the thick black lines illustrate the determination of the NEXAFS onset. (b) Waterfall plot of selected EDCs of the RPES data from the area denoted by the orange box in Fig. 3(d). On the bottom an off-resonant PES spectrum recorded with  $h\nu = 120 \text{ eV}$  is displayed. The energy position of the HOMO and LUMO are indicated by vertical lines.

then a transition from  $|C_i^1 H_{-x}^2 L_0^1\rangle$  to  $|C_i^2 H_{-x}^1 L_0^0\rangle$ . However, if this process led to features intense enough to stick out of the several overlapping Auger signals, these would also have to be present in the data of CuPc/Au(111), since the modifications of the molecular wave functions are known to be relatively small at the investigated interfaces [9]. Since such features are obviously absent in Fig. 3(b), we exclude an explanation involving  $C_i H_{-x} L_0$ -Auger decays.

We must therefore conclude that in the case of the interfaces with ground state charge transfer, a single-particle picture as

defined above is not adequate. Which of the approximations (1)–(4) introduced in section III A fails is not immediately clear. However, since all approximations rely on a small hopping matrix element  $V_{L,M}$  it is quite likely that this assumption is inappropriate here. The finding of a significant hybridization between the metal and molecular states in similar systems corroborates this reasoning [9,10].

The fundamental difference between CuPc/Ag(111) and CuPc/Au(111) is also demonstrated by the comparison of on- and off-resonance EDCs presented in Fig. 4(b). In the case of CuPc/Ag(111) the appearance of the spectra is strongly altered for photon energies in the vicinity of NEXAFS resonance A [see Fig. 4(a)] with respect to the off-resonance spectrum (recorded at 120 eV). This is mainly due to additional features and a generally broadened line shape and is not observed for CuPc/Au(111) (see the respective EDCs in Fig. 4 of Ref. [16] for comparison). An explicit assignment of these additional features is not straightforward, but we take the broad line shape and continuous rise of the background as an indication for the involvement of conduction band states of the Ag(111) substrate in the RPES process through a non-negligible  $V_{L,M}$ . This further supports our statement that a single-particle picture is not sufficient to describe the RPES of such systems, for which very obviously many-body interactions (as, for example, in Refs. [22,23]) need to be taken into account. Note that similar effects are also observed in the RPES data of other molecule-metal interfaces, which show charge transfer in the ground state [28,29].

#### IV. SUMMARY AND CONCLUSION

We demonstrate that based on an explicitly defined single-particle picture and the identification of the responsible decay process, the kinetic energy ( $E_K$ ) of particular constant  $E_K$  features in the resonant photoelectron spectroscopy (RPES) data of molecule-metal interface systems can be successfully calculated for such interfaces which do not show charge transfer in the ground state. If such a charge transfer in the ground state is present, however, we show that this approach is not adequate. In the latter case a significant hybridization between molecular and metal states is reported in literature and also indicated by characteristic changes of the line shape of the RPES data. Hence a single-particle picture, which relies on a small coupling between metallic and molecular states, is limited to systems which only show a weak interaction and no charge transfer in the ground state between molecule and substrate, while otherwise many-body effects have to be adequately taken into account.

#### ACKNOWLEDGMENTS

We thank the BESSY staff, F. Bruckner, S. Gusenleitner, and M. Scholz for support during beamtimes and M. Mulazzi, H. Bentmann, and H. Schwab for stimulating discussions. This work was supported by the Bundesministerium für Bildung und Forschung BMBF (Grant Nos. 05K10WW2 and 03SF0356B) and by the Deutsche Forschungsgemeinschaft DFG (GRK 1221, RE1469/9-1 and SCHO1260/4-1).

- 
- [1] P. A. Brühwiler, O. Karis, and N. Mårtensson, *Rev. Mod. Phys.* **74**, 703 (2002).
  - [2] A. Föhlisch, P. Feulner, F. Hennies, A. Fink, D. Menzel, D. Sanchez-Portal, P. M. Echenique, and W. Wurth, *Nature (London)* **436**, 373 (2005).
  - [3] A. Föhlisch, S. Vijayalakshmi, F. Hennies, W. Wurth, V. Medicherla, and W. Drube, *Chem. Phys. Lett.* **434**, 214 (2007).
  - [4] J. Schnadt, P. A. Bruhwiler, L. Patthey, J. N. O'Shea, S. Sodergren, M. Odellius, R. Ahuja, O. Karis, M. Bassler, P. Persson, H. Siegbahn, S. Lunell, and N. Martensson, *Nature (London)* **418**, 620 (2002).
  - [5] J. B. Taylor, L. C. Mayor, J. C. Swarbrick, J. N. O'Shea, C. Isvoranu, and J. Schnadt, *J. Chem. Phys.* **127**, 134707 (2007).
  - [6] A. J. Britton, A. Rienzo, J. N. O'Shea, and K. Schulte, *J. Chem. Phys.* **133**, 094705 (2010).
  - [7] L. Cao, Y.-Z. Wang, T.-X. Chen, W.-H. Zhang, X.-J. Yu, K. Ibrahim, J.-O. Wang, H.-J. Qian, F.-Q. Xu, D.-C. Qi, and A. T. S. Wee, *J. Chem. Phys.* **135**, 174701 (2011).
  - [8] Y. Zou, L. Kilian, A. Schöll, T. Schmidt, R. Fink, and E. Umbach, *Surf. Sci.* **600**, 1240 (2006).
  - [9] J. Ziroff, F. Forster, A. Schöll, P. Puschnig, and F. Reinert, *Phys. Rev. Lett.* **104**, 233004 (2010).
  - [10] M. Wießner, J. Ziroff, F. Forster, M. Arita, K. Shimada, P. Puschnig, A. Schöll, and F. Reinert, *Nat. Commun.* **4**, 1514 (2013).
  - [11] M. Mugarza, C. Krull, R. Robles, S. Stepanow, G. Ceballos, and P. Gambardella, *Nat. Commun.* **2**, 490 (2011).
  - [12] A. Mugarza, R. Robles, C. Krull, R. Korytár, N. Lorente, and P. Gambardella, *Phys. Rev. B* **85**, 155437 (2012).
  - [13] R. Temirov, A. Lassise, F. B. Anders, and F. S. Tautz, *Nanotechnology* **19**, 1 (2008).
  - [14] J. Ziroff, S. Hame, M. Kochler, A. Bendounan, A. Schöll, and F. Reinert, *Phys. Rev. B* **85**, 161404(R) (2012).
  - [15] M. Häming, L. Weinhardt, A. Schöll, and F. Reinert, *Chem. Phys. Lett.* **510**, 82 (2011).
  - [16] C. Sauer, M. Wießner, A. Schöll, and F. Reinert, *Phys. Rev. B* **89**, 075413 (2014).
  - [17] S. Osborne, A. Ausmees, S. Svensson, A. Kivimäki, O. Sairanen, A. N. de Brito, H. Aksela, and S. Aksela, *J. Chem. Phys.* **102**, 7317 (1995).
  - [18] M. N. Piancastelli, M. Neeb, A. Kivimäki, B. Kempgens, H. M. Köppe, K. Maier, A. M. Bradshaw, and R. F. Fink, *J. Phys. B: At. Mol. Opt. Phys.* **30**, 5677 (1997).
  - [19] M. Neeb, J.-E. Rubensson, M. Biermann, and W. Eberhardt, *J. Electron Spectrosc. and Relat. Phenom.* **67**, 261 (1994).
  - [20] O. Travnikova, C. Miron, M. Bäessler, R. Feifel, M. Piancastelli, S. Sorensen, and S. Svensson, *J. Electron Spectrosc. and Relat. Phenom.* **174**, 100 (2009).
  - [21] C. Sauer, M. Wießner, A. Schöll, and F. Reinert, *New J. Phys.* **17**, 043016 (2015).
  - [22] A. Fujimori and F. Minami, *Phys. Rev. B* **30**, 957 (1984).
  - [23] O. Tjernberg, G. Chiaia, G. Karlsson, and F. de Groot, *J. Phys.: Condens. Matter* **9**, 9863 (1997).

- [24] M. Wießner, N. S. R. Lastra, J. Ziroff, F. Forster, P. Puschnig, L. Dössel, K. Müllen, A. Schöll, and F. Reinert, *New J. Phys.* **14**, 113008 (2012).
- [25] M. L. M. Rocco, M. Haeming, D. R. Batchelor, R. Fink, A. Schöll, and E. Umbach, *J. Chem. Phys.* **129**, 074702 (2008).
- [26] A. Schöll, Y. Zou, T. Schmidt, R. Fink, and E. Umbach, *J. Electron Spectrosc. and Relat. Phenom.* **129**, 1 (2003).
- [27] T. Graber, F. Forster, A. Schöll, and F. Reinert, *Surf. Sci.* **605**, 878 (2011).
- [28] M. Häming, Ph.D. thesis, University of Würzburg (2010).
- [29] A. Bendounan, F. Forster, A. Schöll, D. Batchelor, J. Ziroff, E. Umbach, and F. Reinert, *Surf. Sci.* **601**, 4013 (2007).
- [30] G. A. Sawatzky and J. W. Allen, *Phys. Rev. Lett.* **53**, 2339 (1984).
- [31] J. Zaanen, G. A. Sawatzky, and J. W. Allen, *Phys. Rev. Lett.* **55**, 418 (1985).
- [32] A. Fujimori, F. Minami, and S. Sugano, *Phys. Rev. B* **29**, 5225 (1984).
- [33] A. Kotani and T. Yamazaki, *Prog. Theor. Phys. Supplement* **108**, 117 (1992).
- [34] J. Parlebas, M. Khan, T. Uozumi, K. Okada, and A. Kotani, *J. Electron Spectrosc. Relat. Phenom.* **71**, 117 (1995).
- [35] P. W. Anderson, *Phys. Rev.* **124**, 41 (1961).
- [36] O. Gunnarsson and K. Schönhammer, *Phys. Rev. B* **28**, 4315 (1983).
- [37] J. Stoehr, *NEXAFS Spectroscopy* (Springer-Verlag, Heidelberg, 1992).
- [38] A. Schöll, Y. Zou, L. Kilian, D. Hübner, D. Gador, C. Jung, S. G. Urquhart, T. Schmidt, R. Fink, and E. Umbach, *Phys. Rev. Lett.* **93**, 146406 (2004).
- [39] H. Oji, R. Mitsumoto, E. Ito, H. Ishii, Y. Ouchi, K. Seki, T. Yokoyama, T. Ohta, and N. Kosugi, *J. Chem. Phys.* **109**, 10409 (1998).
- [40] M. Wießner, Ph.D. thesis, University of Würzburg (2013).
- [41] S. Kera, M. B. Casu, A. Schoell, T. Schmidt, D. Batchelor, E. Ruehl, and E. Umbach, *J. Chem. Phys.* **125**, 014705 (2006).
- [42] M. Häming, C. Scheuermann, A. Schöll, F. Reinert, and E. Umbach, *J. Electron Spectrosc. Relat. Phenom.* **174**, 59 (2009).